Chimica Techno Acta
published by Ural Federal University
eISSN 2411-1414
chimicatechnoacta.ru

ARTICLE
2026, vol. 13(1), No. 9253
DOI: 10.15826/chimtech.9253

Comparative study of medium-pore zeolites (ZSM-5, ZSM-23, ZSM-48) and SAPO-11 in the hydroisomerization of *n*-hexadecane

Dmitry Serebrennikov [a] *, Artur Malunov [a], Nadezhda Filippova [a], Denis Sabirov [a], Alfira Khazipova [a], Vladimir Gus'kov [b], Marat Agliullin [a]

a: Institute of Petrochemistry and Catalysis, Ufa Federal Research Centre of the Russian Academy of Sciences, Ufa 450075, Russia
b: Faculty of Science and Technology, Ufa University of Science and Technology, Ufa 450076, Russia
* Corresponding author: d25c25@yandex.ru

Abstract

The high selectivity of bifunctional catalysts in the hydroisomerization of long-chain n-paraffins is a key factor for producing high-quality fuels. However, it is directly dependent on a complex balance between the topology, acidity, morphology, and crystal size of the zeolite support. To address this challenge, this work presents a comparative study of medium-pore molecular sieves (ZSM-5, ZSM-23, ZSM-48, and SAPO-11) with different structural and acidic properties. The physicochemical characteristics of the materials were investigated using a set of analytical techniques, including XRD, SEM, low-temperature N_2 adsorption, and NH_3-TPD. It was shown that the pore topology (3D in ZSM-5 vs. 1D in the others), chemical composition, and crystal morphology (ranging from ~50 nm nanoprisms for ZSM-48 to 200–300 nm needles for ZSM-23-80 and 1 μm needles for ZSM-23-100) determine both the textural properties and the strength and concentration of acid sites. In the hydroisomerization of n-hexadecane, the Pt/ZSM-5 catalyst, with its high concentration of strong acid sites and 3D channel pore structure, exhibited the highest activity but an extremely low isomer selectivity (<7%) due to intense cracking. The best results were demonstrated by the Pt/SAPO-11 and Pt/ZSM-48 samples, which provided isomer yields of 80% and 73%, respectively. Their high efficiency is attributed to the combination of a one-dimensional pore structure, moderate acidity, and nanocrystalline size, which minimizes diffusion limitations and suppresses side reactions. Thus, controlling the topology and acidity in combination with nanocrystalline morphology is an effective strategy for the rational design of highly selective hydroisomerization catalysts.

Key findings

- The highest isomer yields (80% and 73%) were achieved with Pt/SAPO-11 and Pt/ZSM-48, which is attributed to the combination of moderate acidity, nanocrystalline size, and one-dimensional pore channels.
- The three-dimensional pore structure of Pt/ZSM-5 leads to intense cracking and low isomer selectivity (<7%) due to its high acidity and lack of spatial constraints.
- The Pt/ZSM-23-80 catalyst, featuring the strongest acid sites, is effective for low-temperature isomerization; however, its needle-like crystal morphology limits selectivity compared to nanocrystalline analogues.

Accompanying information

Article history
Received: 03.11.25
Revised: 21.11.25
Accepted: 24.11.25
Available online: 04.12.25

Keywords
Molecular sieves; zeolites; silicoaluminophosphates; hydroisomerization of n-paraffins; bifunctional catalysts

Funding
The work was performed within the framework of the state task of the IPC UFRC RAS (topic No.FMRS-2024-0012 "Bifunctional Molecular-Sieve Catalytic Systems for the Production of Low-Pour-Point Diesel Fuels".

Supplementary information
Transparent peer review: READ

Sustainable Development Goals
9 INDUSTRY, INNOVATION AND INFRASTRUCTURE

1. Introduction

The modern oil refining industry faces the necessity of simultaneously improving the quality of diesel fuels and reducing their environmental impact. A key challenge is the enhancement of low-temperature properties through the catalytic hydroisomerization of long-chain n-paraffins (C_{14}–C_{20}). Despite their high cetane number, these compounds exhibit unacceptably high pour and cloud points [1,2]. An effective solution to this problem is the selective conversion of linear paraffins into branched isomers—preferably monomethyl-substituted ones—which retain a high cetane number while demonstrating significantly lower pour points [3–5].

The central scientific challenge remains the minimization of undesirable hydrocracking, which reduces the yield of the target diesel component and negatively impacts process economics [6]. The most promising catalysts for this task are bifunctional systems that combine a noble metal (typically Pt) with an acidic support based on 10-membered ring (10-MR) molecular sieves. Their micropores (with a diameter of ~5 Å) are comparable to the size of higher paraffin molecules, enabling a shape-selective effect, suppressing the formation of bulky, multibranched carbenium ions that lead to cracking, and favoring the formation of less bulky monobranched isomers [7–9].

The most frequently discussed 10-MR materials for hydroisomerization in the literature are ZSM-23 (MTT), ZSM-48 (RFE), ZSM-22 (TON), and SAPO-11 (AEL). All of them are characterized by a one-dimensional (1D) system of non-intersecting micropores, which theoretically ensures high selectivity. Differences in their catalytic behavior are traditionally explained by subtle variations in channel topology, pore geometry (ranging from elliptical 3.9×6.5 Å in SAPO-11 to the more isometric 5.3×5.6 Å in ZSM-48), and the nature of the acid sites—strong Brønsted acids in aluminosilicates and moderate ones in silicoaluminophosphates [10–14].

However, despite the extensive literature [15–19], comparative studies of these materials often suffer from a lack of a systematic approach. Firstly, many studies utilize commercial or standardly synthesized samples without detailed characterization of their morphology. This is a significant omission, as even when using "standard" protocols, the crystal size and shape can vary substantially depending on the gel composition, crystallization temperature, synthesis time, and other factors. Secondly, even when the materials exhibit high dispersity, differences in morphology are rarely considered as a significant parameter influencing the catalytic properties. Instead, the focus is placed exclusively on topology, pore size, and acidity, leading to an incomplete or distorted understanding of the reasons behind the differences in activity and selectivity.

Meanwhile, according to modern understanding of heterogeneous catalysis in microporous materials, crystal morphology plays a decisive role in the process efficiency [20]. Even with identical porosity and acidity, the size and shape of the crystallites determine the length of the diffusion pathways, and, consequently, the uniformity of the reaction distribution, the residence time of intermediates within the pores, and the likelihood of secondary transformations, including hydrocracking [21–23]. Thus, two catalysts with identical topology and acidity but different morphology can exhibit fundamentally different catalytic behavior.

It is precisely this systematic shortcoming that we aim to address in the present work. We do not resort to exotic or poorly reproducible synthesis methods but instead employ well-known, standard protocols, which ensure high reproducibility and practical relevance of the obtained results. However, unlike most publications, we deliberately select a set of materials that allows for a clear demonstration of the influence of morphology on catalytic properties, while maintaining control over other variables.

The study includes a series of molecular sieves of different structural types: ZSM-5 (MFI), ZSM-23 (MTT), ZSM-48 (RFE), and SAPO-11 (AEL). All of them were synthesized using established literature methods, which ensure the production of highly dispersed materials. However, as our characterization has shown, the crystal morphology differs significantly, ranging from isometric particles of SAPO-11 to elongated needles of ZSM-23. In contrast, ZSM-5 with a three-dimensional pore system but with acidity similar to ZSM-23 was selected, allowing for the assessment of the contribution of topology independently of the acid properties.

An equally important aspect of our approach was the inclusion of two ZSM-23 samples for comparison: one with high dispersity and moderate acidity, and the other with significantly larger crystals and a reduced concentration of acid centers (achieved by increasing the SiO_2/Al_2O_3 ratio and the dilution of the reaction gel with water). This allowed us to decouple the influences of morphology and acidity.

Thus, the present work is dedicated to a systematic, balanced comparative analysis that clearly reveals the contribution of crystal morphology to the catalytic performance in the hydroisomerization of n-hexadecane—a model compound representing the diesel fraction. We demonstrate that even when using standard syntheses and in the presence of high dispersity, differences in crystal shape and size can be decisive for selectivity, and that ignoring this factor leads to erroneous interpretations.

All the catalysts were characterized using a unified set of techniques (X-ray diffraction, scanning electron microscopy, ammonia temperature-programmed desorption, nitrogen adsorption) and tested under identical reaction conditions.

 DOI: 10.15826/chimtech.9253

2. Materials and methods

2.1. Synthesis of ZSM-5 zeolite

ZSM-5 zeolite with an SiO_2/Al_2O_3 ratio of 50 was synthesized from a reaction gel of the following molar composition: $0.03Na_2O{\cdot}0.04TBAB{\cdot}0.02Al_2O_3{\cdot}1.00SiO_2{\cdot}30H_2O$. Sodium hydroxide (NaOH), silica sol (40% SiO_2, Prom-Steklo), sodium aluminate (Sigma-Aldrich) as sources of silicon and aluminum, respectively, with tetrabutylammonium bromide (TBAB, Sigma-Aldrich) as the template.

The reaction gel was prepared by adding an aqueous NaOH solution and distilled water to a calculated amount of silica sol under vigorous stirring. Subsequently, aqueous solutions of the template (TBAB) and aluminum nitrate were added sequentially to the resulting mixture.

After mixing all components, the resulting gel was transferred into a Teflon-lined autoclave and subjected to hydrothermal crystallization at 160 °C for 48 h. The solid product was recovered by centrifugation and repeatedly washed with distilled water until the washings reached neutral pH. Finally, the samples were dried at 150 °C for 8–10 h.

2.2. Synthesis of ZSM-23 zeolite

ZSM-23 zeolite with a SiO_2/Al_2O_3 ratio of 80 was synthesized from a reaction gel of the following molar composition: $0.35Na_2O{\cdot}0.0125Al_2O_3{\cdot}1.00SiO_2{\cdot}0.7DMF{\cdot}35H_2O$. Sodium hydroxide (NaOH), silica sol (40% SiO_2, Ludox AS-40), aluminum nitrate nonahydrate ($Al(NO_3)_3{\cdot}9H_2O$, 99%, Acros Organics), and dimethylformamide (DMF, 99%, Acros Organics) were used for its preparation.

The reaction gel was prepared by adding NaOH and distilled water to a calculated amount of SiO_2 sol under vigorous stirring. A calculated amount of the template and $Al(NO_3)_3{\cdot}9H_2O$ was added to the resulting solution. Subsequently, DMF was added sequentially to the resulting mixture.

After mixing all components, the resulting gels were aged at 60 °C for 24 h and then crystallized at 170 °C for 72 h. The solid products were separated by centrifugation and washed with distilled water until the washings reached neutral pH.

ZSM-23 zeolite with a SiO_2/Al_2O_3 ratio of 100 was synthesized using an analogous procedure from a reaction gel of the following molar composition: $0.35Na_2O{\cdot}0.01Al_2O_3{\cdot}1.00SiO_2{\cdot}0.7DMF{\cdot}45H_2O$.

2.3. Synthesis of ZSM-48 zeolite

ZSM-48 zeolite with a SiO_2/Al_2O_3 ratio of 150 was synthesized from a reaction gel of the following molar composition: $0.08Na_2O{\cdot}0.0067\ Al_2O_3{\cdot}1.00SiO_2{\cdot}0.06HMB{\cdot}25H_2O$. Sodium hydroxide (NaOH), silica sol (40% SiO_2, Prom-Steklo), sodium aluminate (Sigma-Aldrich), and hexamethonium bromide (HMB, Sigma-Aldrich) were used as the template.

The reaction gel was prepared by adding NaOH and distilled water to a calculated amount of silica sol under vigorous stirring. A calculated amount of the template and sodium aluminate was added to the resulting solution. Subsequently, HMB was added sequentially to the resulting mixture.

After mixing all components, the resulting gel was transferred into a stainless-steel autoclave and subjected to hydrothermal crystallization at 160 °C for 96 h. The solid product was recovered by centrifugation, thoroughly washed with distilled water until neutral pH was reached, and dried at 110 °C.

2.4. Synthesis of silicoaluminophosphate SAPO-11

Silicoaluminophosphate molecular sieves of the SAPO-11 type were synthesized from reaction gels with the following molar composition: $1.0Al_2O_3{\cdot}1.0P_2O_5{\cdot}0.1SiO_2{\cdot}1.0(DPA){\cdot}40H_2O$. Aluminum isopropoxide (IPA, 99%, Acros Organics) was used as the aluminum source. The sources of phosphorus and silicon were orthophosphoric acid, H_3PO_4 (85%, Reakhim), and a silica sol prepared from tetraethyl orthosilicate (TEOS, 99%, Ekos) according to the procedure described in [24]. Di-n-propylamine (DPA, 99%, Acros Organics) was used as the template.

After the addition of all components, the mixture was stirred vigorously for 1 h until a homogeneous gel was obtained, which was then aged in a thermostat at 90 °C for 24 h. The resulting aged gels were loaded into a stainless-steel autoclave with a special PTFE liner and crystallized at 200 °C for 24 h. After crystallization, the SAPO-11 samples were washed with distilled water to neutral pH, separated by centrifugation, and dried at 90 °C for 24 h.

2.5. Catalyst preparation

The H-form of the zeolite samples was obtained after crystallization via ion exchange of Na^+ cations with NH_4^+ cations in an aqueous solution of ammonium nitrate (NH_4NO_3, 98%, Reakhim) at 70 °C for 1 h under stirring. The resulting suspension was then dried at 120 °C and calcined at 550 °C for 4 h in an air atmosphere. The samples in the H-form were assigned an H-index.

The calcined and powdered molecular sieve samples (in the H-form) were first pressed into pellets, then crushed and sieved to collect the 0.1–0.2 mm fraction. This fraction was calcined in an air atmosphere at 600 °C for 6 h. The calcined support was impregnated by the incipient wetness method with an aqueous solution of $H_2PtCl_6{\cdot}6H_2O$ to achieve a Pt loading of 0.5 wt.% relative to the support mass. The impregnated sample was dried at 100 °C for 24 h and then calcined at 550 °C for 5 h. Prior to the reaction, the catalyst was reduced in a hydrogen flow at 400 °C and 30 bar for 14 h. The Pt-containing samples were subsequently assigned a "Pt"- index.

 DOI: 10.15826/chimtech.9253

2.6. Material analysis methods

The chemical composition of the synthesized molecular sieves was determined by energy-dispersive X-ray fluorescence spectroscopy using a Shimadzu EDX-7000P spectrometer (Shimadzu Corporation, Germany) and the fundamental parameters method.

The phase composition of the zeolites was analyzed using a Shimadzu XRD-7000 diffractometer with Cu Kα radiation. Scanning was performed over a 2θ range from 3° to 40° with a scan rate of 1°/min. The X-ray diffraction data were processed using Shimadzu XRD software with the PDF2 database for phase analysis. Crystallinity was assessed based on the content of the amorphous halo, which was measured in the 2θ range of 20 to 30 degrees using the Shimadzu XRD Crystallinity software. The degree of crystallinity was calculated as the ratio of the total integral intensity of the crystalline phase to the sum of the total integral intensities of the crystalline and amorphous phases.

The morphology and crystal size of the synthesized molecular sieves were determined by field-emission scanning electron microscopy (FE-SEM) using a Hitachi Regulus SU8220 scanning electron microscope. Images were acquired in secondary electron mode at an accelerating voltage of 2 kV.

The textural characteristics of the samples, previously calcined in air (600°C, 6 h), were investigated by low-temperature nitrogen adsorption-desorption at 77 K using an Altamira Instruments QUICK-200 analyzer. The specific surface area was calculated using the Brunauer–Emmett–Teller (BET) method. The micropore volume was evaluated using the t-plot method, and the mesopore size distribution was determined using the Barrett–Joyner–Halenda (BJH) model applied to the desorption branch of the isotherm.

The acidic properties were evaluated by temperature-programmed desorption of ammonia (NH_3-TPD) using an Altamira AMI-400TPx instrument. The calcined samples were subjected to pre-treatment at 550 °C in a helium flow for 2 h. Subsequently, a 10 vol.% mixture of NH_3 in helium was introduced to the samples at 100 °C for 30 min. The samples were then purged with helium to remove physically adsorbed ammonia. The desorption of NH_3 was monitored over a temperature range from 100 to 600 °C with a heating rate of 10 °C/min. The resulting TPD profiles were deconvoluted into individual Gaussian peaks, and the acid site concentrations were determined by integrating the areas of the deconvoluted components. Peaks exhibiting maxima within the temperature ranges of 100–250 °C, 250–400 °C, and 400–600 °C were assigned to weak, medium, and strong acid sites, respectively. Desorption activation energies (225, 215, and 208 kJ/mol) were calculated using Catalyst Characterization Instruments software (v1.0.0.183) based on the dependence of the peak maximum temperature on the heating rate, in accordance with the Redhead analysis for first-order desorption kinetics [25].

The platinum dispersion and average particle size in the Pt-containing samples were determined by pulse chemisorption of hydrogen using an Altamira AMI-400TPx instrument. Prior to analysis, the samples were reduced in a hydrogen flow at 400 °C. Chemisorption measurements were carried out at 40 °C. Platinum dispersion and mean particle diameter were calculated from the amount of adsorbed hydrogen using Catalyst Characterization Instrument software, assuming a hydrogen-to-platinum stoichiometry (H:Pt) of 1:1.

2.7. Catalytic testing in n-hexadecane hydroisomerization

The tests of Pt-containing samples were carried out on a laboratory setup equipped with a continuous-flow isothermal reactor with a fixed catalyst bed, at temperatures ranging from 220 °C to 340 °C. The reactor pressure was maintained at 30 bar. The hydrogen-to-hydrocarbon molar ratio was 10 mol/mol, and the weight hourly space velocity (WHSV) was 2 h^{-1}.

The reaction products were analyzed by gas-liquid chromatography using a Chromatek Crystal-5000 chromatograph equipped with a flame ionization detector (FID) and a 50 m glass capillary column (100% dimethylpolysiloxane, 50 m × 0.2 mm, 0.5 μm). Product identification was performed by gas chromatography-mass spectrometry (GC-MS) in the electron impact ionization mode (ion source temperature 200 °C, ionization energy 70 eV) using a Shimadzu instrument. The chromatograph was equipped with a 50-meter DB-5ms column (stationary phase: (5%-phenyl)-methylpolysiloxane), and the Wiley (NIST 2011) mass spectral database was used for identification.

3. Results and Discussion

As can be seen from the presented diffractograms (Figure 1), all the samples exhibit sharp and intense diffraction peaks characteristic of their respective crystal structures. The absence of extraneous reflections indicates the high phase purity of the synthesized materials, while the narrow and well-resolved peaks attest to a high degree of crystallinity.

The positions and relative intensities of the diffraction maxima for each sample are in excellent agreement with the reference data from the PDF (Powder Diffraction File) database: ZSM-5 (PDF No. 00-043-0321), ZSM-23 (PDF No. 00-044-0102), ZSM-48 (PDF No. 00-043-0531), and SAPO-11 (PDF No. 00-041-0023). The observed match confirms not only the identity of the synthesized phases with their theoretical structures but also the absence of significant lattice distortions or the formation of impurity phases during synthesis. The crystallinity for all samples exceeded 90% (Table 1).

 DOI: 10.15826/chimtech.9253

Figure 2 shows the morphology and crystal size of the synthesized molecular sieves according to scanning electron microscopy (SEM) data. The ZSM-5 sample consists of well-defined prismatic crystals with characteristic facets typical of the orthorhombic modification of this zeolite. The crystal sizes range from 200 to 500 nm, and the particles show a moderate level of aggregation, indicating controlled growth during synthesis. This morphology is favorable for catalytic applications as it combines a developed external surface area with the preservation of the microporous structure.

The ZSM-23-80 crystals exhibit a distinct needle-like (or fibrous) morphology, with a length of 200–300 nm and a high aspect ratio.

This shape is characteristic of zeolites with a one-dimensional pore system and can promote the directed diffusion of reagents along the channels. However, it also increases the risk of undesirable hydrocracking side reactions due to the prolonged residence time of intermediates within the channels.

For a more detailed comparison of the influence of morphology on catalytic properties, a ZSM-23-100 sample with larger needle-like crystals approximately 1 μm in length was additionally synthesized. Compared to ZSM-23-80, the longer diffusion path in the larger ZSM-23-100 crystals may further increase the residence time of intermediates in the channels, thereby additionally enhancing the likelihood of side reactions such as hydrocracking.

In the case of ZSM-48, small prismatic crystals with a characteristic size of approximately 50 nm are observed. The nanocrystals of this phase possess a significantly increased external surface area compared to larger analogues, which can positively affect the accessibility of active sites and reduce diffusion limitations.

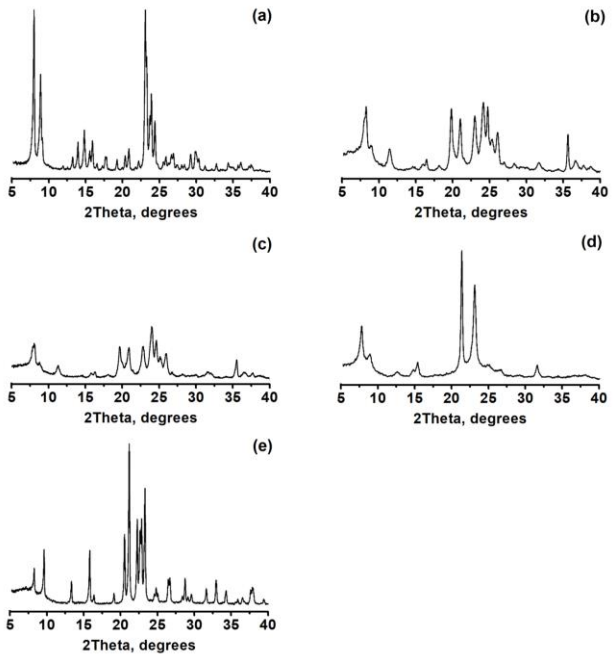

Figure 1 X-ray diffractograms of crystalline molecular sieves: (a) ZSM-5; (b) ZSM-23-80; (c) ZSM-23-100; (d) ZSM-48; (e) SAPO-11.

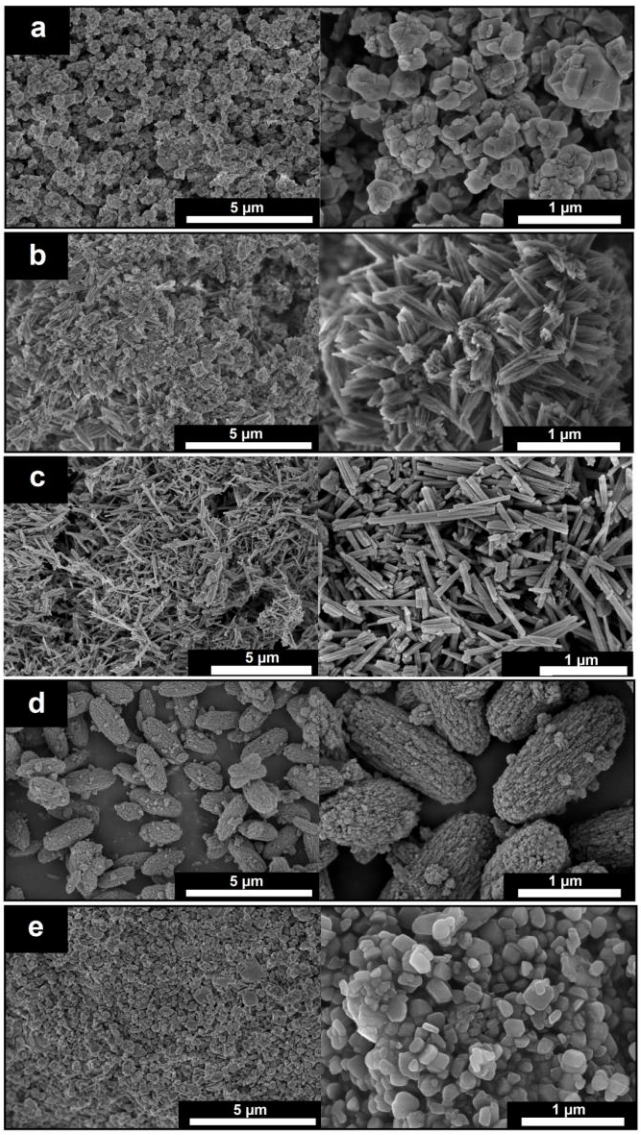

Figure 2 SEM micrographs of molecular sieve samples of different structural types: (a) ZSM-5; (b) ZSM-23-80; (c) ZSM-23-100; (d) ZSM-48; (e) SAPO-11.

Table 1 Chemical and phase composition of molecular sieves of different structural types.

Sample	Chemical composition	Phase	DR*
ZSM-5	$0.019Al_2O_3{\cdot}1.000SiO_2$	MFI	93
ZSM-23-80	$0.013Al_2O_3{\cdot}1.000SiO_2$	MTT	94
ZSM-23-100	$0.010Al_2O_3{\cdot}1.000SiO_2$	MTT	92
ZSM-48	$0.007Al_2O_3{\cdot}1.000SiO_2$	RFE	91
SAPO-11	$1.000\ Al_2O_3{\cdot}0.018SiO_2$	AEL	93

* DR – degree of crystallinity, %

The silicoaluminophosphate SAPO-11 consists of crystals ranging in size from 100 to 300 nm with a morphology resembling truncated cube-like cones, partially forming aggregates. This shape can facilitate effective mass transfer in reactions involving bulky molecules, such as in the hydroisomerization of C_{16+} paraffins.

The textural properties of the synthesized molecular sieves were studied by low-temperature nitrogen adsorption-desorption. The obtained isotherms (Figure 3) are classified as type IV according to the IUPAC classification, indicating a mixed microporous and mesoporous structure

 DOI: 10.15826/chimtech.9253

of the samples. The presence of a distinct hysteresis loop in the relative pressure range P/P_0 from 0.4 to 0.9 confirms the presence of mesopores.

Pore size distribution calculations performed using the BJH method revealed the presence of mesopores in the range of 2–20 nm for all materials. These pores likely represent intercrystalline voids formed due to the aggregation of nanocrystals, which is consistent with the scanning electron microscopy (SEM) data. It should be noted that the peak in the ~2 nm region on the BJH curves is an artifact associated with the tensile strength effect of nitrogen and was not considered in the quantitative porosity analysis.

The quantitative textural characteristics of the samples are presented in Table 2. Analysis of the parameters related to microporosity reveals a clear dependence on the type of crystal structure.

The ZSM-5 zeolite possesses the most developed microporous structure, which is reflected in the maximum values of both the BET specific surface area (S_{BET}) and the micropore volume (V_{micro}). This is an expected result, due to its three-dimensional system of intersecting channels (MFI structural type) and high degree of crystallinity. SAPO-11 (AEL type) is characterized by somewhat lower but comparable values, whereas the zeolites ZSM-48 and ZSM-23-80 with a one-dimensional pore system (RFE and MTT, respectively) exhibit significantly lower S_{BET} and V_{micro} values.

Conversely, the analysis of parameters characterizing secondary porosity (intercrystalline space) reveals a different trend, which depends more significantly on crystal morphology and packing mode. The largest mesopore volume (V_{meso}) is observed for SAPO-11 and ZSM-23-80. This can be explained by their morphology: the SAPO-11 nanocrystals with a truncated cone shape and the needle-like ZSM-23-80 crystals tend to form loose packing with significant intercrystalline voids.

Table 2 Pore structure characteristics of molecular sieves of different structural types.

Sample	S_{BET}, m²/g	S_{EX}, m²/g	V_{micro}, cm³/g	V_{meso}, cm³/g
H-ZSM-5	416	127	0.11	0.09
H-ZSM-23-80	198	72	0.05	0.16
H-ZSM-23-100	132	39	0.04	0.08
H-ZSM-48	201	75	0.05	0.12
SAPO-11	228	54	0.07	0.17

S_{BET} - specific surface according to BET;
S_{EX} - external specific surface area;
V_{micro} - specific volume of micropores;
V_{meso} - specific volume of mesopores.

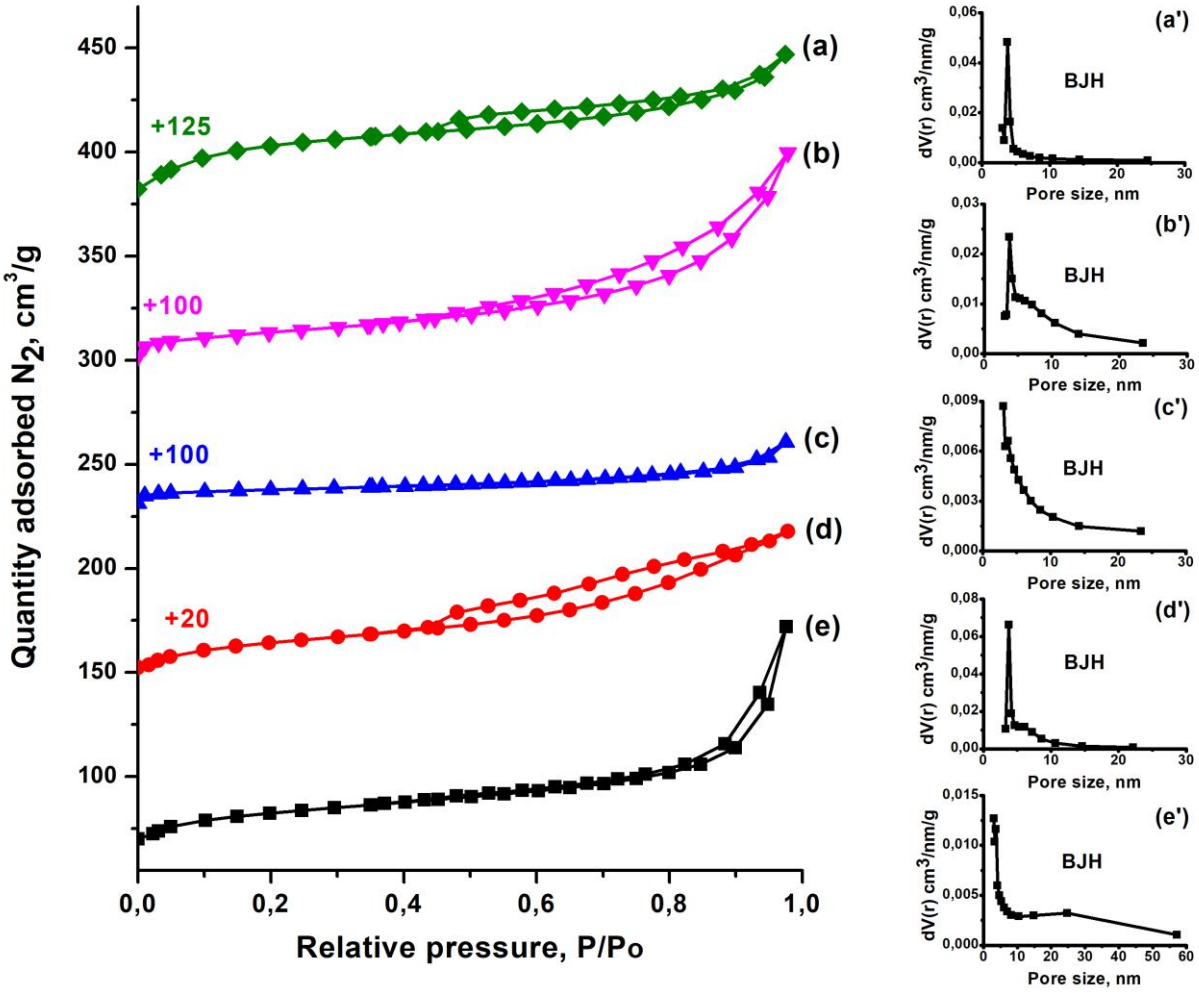

Figure 3 Nitrogen adsorption-desorption isotherms (a-e) and pore size distributions (a'-e') of molecular sieve samples of different structural types: (a, a') – ZSM-5; (b, b') – ZSM-23-80; (c, c') – ZSM-23-100; (d, d') – ZSM-48; (e, e') – SAPO-11.

 DOI: 10.15826/chimtech.9253

In contrast, ZSM-5, despite having the highest external specific surface area (S_{EX}), possesses the smallest mesopore volume. This is due to the low degree of intergrowth between its nanocrystals. ZSM-48, composed of nano-sized prisms, occupies an intermediate position in terms of mesopore volume, indicating a moderate packing density of its crystallites.

It should be noted that among all the studied samples, ZSM-23-100 exhibits the least pronounced hysteresis loop. This is consistent with its larger needle-like crystals, approximately 1 μm in length, which form denser packing compared to the nanocrystalline ZSM-23-80. Accordingly, the values of the BET specific surface area, external surface area, micropore volume, and mesopore volume for ZSM-23-100 are the lowest among the studied molecular sieve samples.

The acidic properties of the synthesized materials were studied by temperature-programmed desorption of ammonia (NH_3-TPD) (Figure 4)

Analysis of the total acidity revealed a direct correlation between the number of acid sites and the aluminum content in the zeolite framework (Table 3). The maximum concentration of sites was recorded for H-ZSM-5 with a SiO_2/Al_2O_3 ratio of 49. As this ratio increases in the series H-ZSM-23-80 (SiO_2/Al_2O_3 = 76) and H-ZSM-48 (SiO_2/Al_2O_3 = 143), the total acidity consistently decreases. The lowest number of acid sites is demonstrated by SAPO-11, which is expected for silicoaluminophosphates, where acidity arises from the limited isomorphic substitution of silicon in the phosphate matrix, and the concentration of such sites is typically lower than in aluminosilicate zeolites.

The distribution of sites by strength reveals a more complex picture. Although H-ZSM-5 leads in the number of both medium-strength and strong acid sites, and SAPO-11 is at the bottom of the list in terms of the number of strong sites, an interesting feature is observed: SAPO-11 contains more medium-strength sites than H-ZSM-48, despite its lower overall acidity. This may indicate that at a very high silica-to-alumina ratio in H-ZSM-48, the remaining acid sites are predominantly weak or partially inaccessible to ammonia molecules.

The most important insights are derived from the analysis of acid site strength, assessed by the temperature of the ammonia desorption peak maximum. A non-trivial dependence is observed here: the strongest acid sites were found not in H-ZSM-5, but in H-ZSM-23-80. This effect can be explained by the strong diffusion constraints within the 1D-10R channels, caused by the high aspect ratio of the elongated needle-like crystals, which leads to higher-temperature ammonia desorption. In H-ZSM-5, despite their larger total number, the strength of the sites, according to NH_3-TPD data, appears somewhat lower due to both its lower silica-to-alumina ratio and better diffusion within the three-dimensional system of 10R channels.

The H-ZSM-23-100 sample, which possesses the largest crystals among all the studied molecular sieve samples (length ~1 μm) and an increased molar SiO_2/Al_2O_3 ratio of 95, exhibits a lower concentration of acid sites compared to H-ZSM-23-80 (SiO_2/Al_2O_3 = 76). Consequently, the total concentration of acid sites in H-ZSM-23-100 turned out to be comparable to that of H-ZSM-48—the sample with the highest SiO_2/Al_2O_3 ratio of 143 in the series.

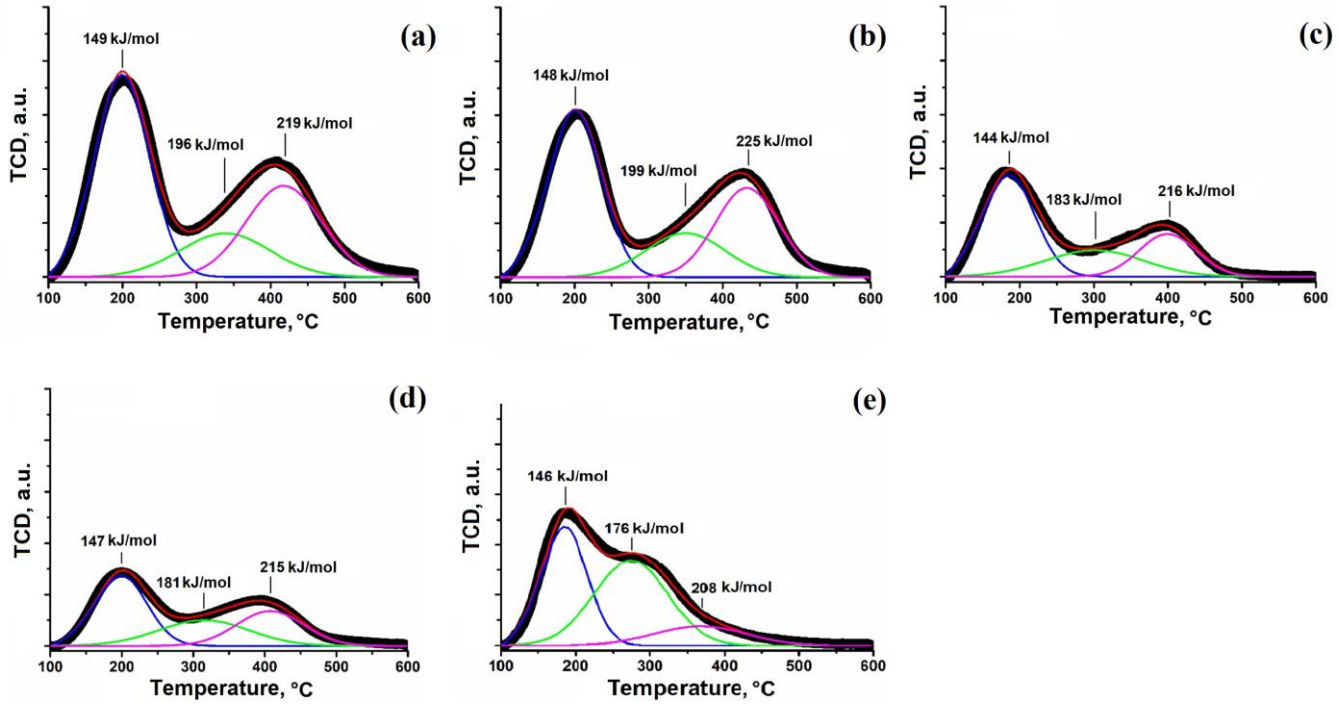

Figure 4 NH_3-TPD profiles for molecular sieve samples of different structural types: H-ZSM-5 (a); H-ZSM-23-80 (b); H-ZSM-23-100 (c); H-ZSM-48 (d); SAPO-11 (e).

 DOI: 10.15826/chimtech.9253

Table 3 Acidic properties of molecular sieve samples of different structural types according to NH_3-TPD data.

Sample	SiO_2/Al_2O_3	Acidity by NH_3 TPD, μmol/g			
		Weak[a]	Moderate[b]	Strong[c]	Σ
H-ZSM-5	49	256	94	166	516
H-ZSM-23-80	76	206	85	139	430
H-ZSM-23-100	95	125	63	60	248
H-ZSM-48	143	92	61	62	215
SAPO-11	0.1	134	159	45	338

[a] the amount of ammonia desorbed in the range of 100–250 °C;
[b] the amount of ammonia desorbed in the range of 250–400 °C;
[c] the amount of ammonia desorbed in the range of 400–600 °C;

However, unlike H-ZSM-23-80, which exhibits increased acid site strength, the strength of the acid sites in H-ZSM-23-100 proved to be comparable to H-ZSM-48 and significantly lower than that of H-ZSM-23-80. This is likely due to the fact that the increased crystal size in H-ZSM-23-100, while preserving the one-dimensional pore structure, simultaneously reduces the density of acid sites and weakens their mutual influence, while also diminishing the contribution of diffusion effects to the shift in ammonia desorption temperature. Thus, despite having morphology similar to H-ZSM-23-80, H-ZSM-23-100 exhibits acid properties closer to the "high-silica" H-ZSM-48 both in terms of acid site concentration and their strength.

Thus, the acidic properties of the studied molecular sieves are governed by several factors: the chemical nature of the framework, the concentration of heteroatoms, their degree of isolation, and the characteristics of the channel pore system. In this context, H-ZSM-5 stands out due to its high concentration of acid sites, making it a universal catalyst for a wide range of processes.

H-ZSM-23-80, while having a lower number of sites, possesses the strongest ones, which can be critically important for reactions that require lower process temperatures. H-ZSM-48 is characterized by limited acidity, both in terms of the number and strength of sites, whereas SAPO-11 exhibits moderate and relatively weak acidity. This property is often exploited to achieve high selectivity in processes where strong acidity leads to undesirable side reactions, such as in the isomerization of *n*-paraffins.

Previous studies have shown that loading 0.5 wt.% Pt provides a sufficient number of hydrogenation-dehydrogenation sites, and the limiting step in the hydroisomerization of n-hexadecane becomes the transformation occurring at the acid sites of the support [26].

Hydrogen chemisorption measurements of platinum supported on various molecular sieves (Table 4) reveal a dependence of Pt dispersion and particle size on the properties of the support. Platinum dispersion ranges from 18% to 37%, corresponding to average particle sizes between 5.6 nm and 2.7 nm, respectively.

Table 4 Dispersion and particle size of Pt in Pt-containing samples obtained by H_2 chemisorption.

Sample	Pt dispersion, %	Pt particle size, nm
Pt/ZSM-5	37	2.7
Pt/ZSM-23-80	30	3.3
Pt/ZSM-23-100	18	5.6
Pt/ZSM-48	24	4.1
Pt/SAPO-11	26	3.8

X-ray fluorescence spectroscopy confirmed that the Pt loading in all samples was close to the target value (~0.5 wt.%). The highest Pt dispersions were obtained on ZSM-5 and ZSM-23-80 supports that possess the highest concentration of acidic sites, which likely contributes to the stabilization of small Pt particles through enhanced metal–support interactions. In contrast, ZSM-23-100, characterized by significantly larger crystals compared to the other supports, exhibited the lowest dispersion and the largest Pt particles, suggesting that crystal size (and consequently external surface area and accessibility) plays an important role in metal distribution.

The catalyst based on H-ZSM-5 exhibited the highest overall activity in the hydroconversion of n-hexadecane (Figure 5). This is explained by the combination of its high concentration of acid sites, significant specific surface area, and developed microporosity of its three-dimensional MFI structure. Furthermore, the prismatic ZSM-5 crystals, 200–500 nm in size, provide sufficient external surface area and higher accessibility to the acid sites.

However, this very combination of properties—especially the high concentration of strong acid sites and the three-dimensional channel pore structure—leads to the rapid secondary cracking of the formed branched isomers. As a result, despite the high conversion, the yield of the target isomers is the lowest, and the selectivity drops sharply even at moderate conversion levels. The main reaction products over the Pt/ZSM-5 catalyst are cracking products, predominantly C_3-C_{13} hydrocarbons.

The main reaction products for catalysts based on 1D-10R molecular sieves are mono- and dimethyl-substituted C_{16} isomers, predominantly 2-, 3-, and 6-monomethylpentadecanes, as well as 2,12- and 2,6-dimethyltetradecanes. As the temperature increases, the conversion of n-hexadecane rises, but the selectivity towards C_{16} isomers decreases due to the enhanced side reaction of hydrocracking. Consequently, the yield of the target isomers passes through a maximum (Figure 5).

It is particularly noteworthy that among the aluminosilicate zeolites, ZSM-48 demonstrated the best performance, achieving an isomer yield of 73%. This result significantly surpasses both ZSM-23-80 (55%) and especially ZSM-5, for which the maximum isomer yield was only 7%. This behavior of ZSM-48 can be explained by the unique combination of its structural and acidic characteristics.

 DOI: 10.15826/chimtech.9253

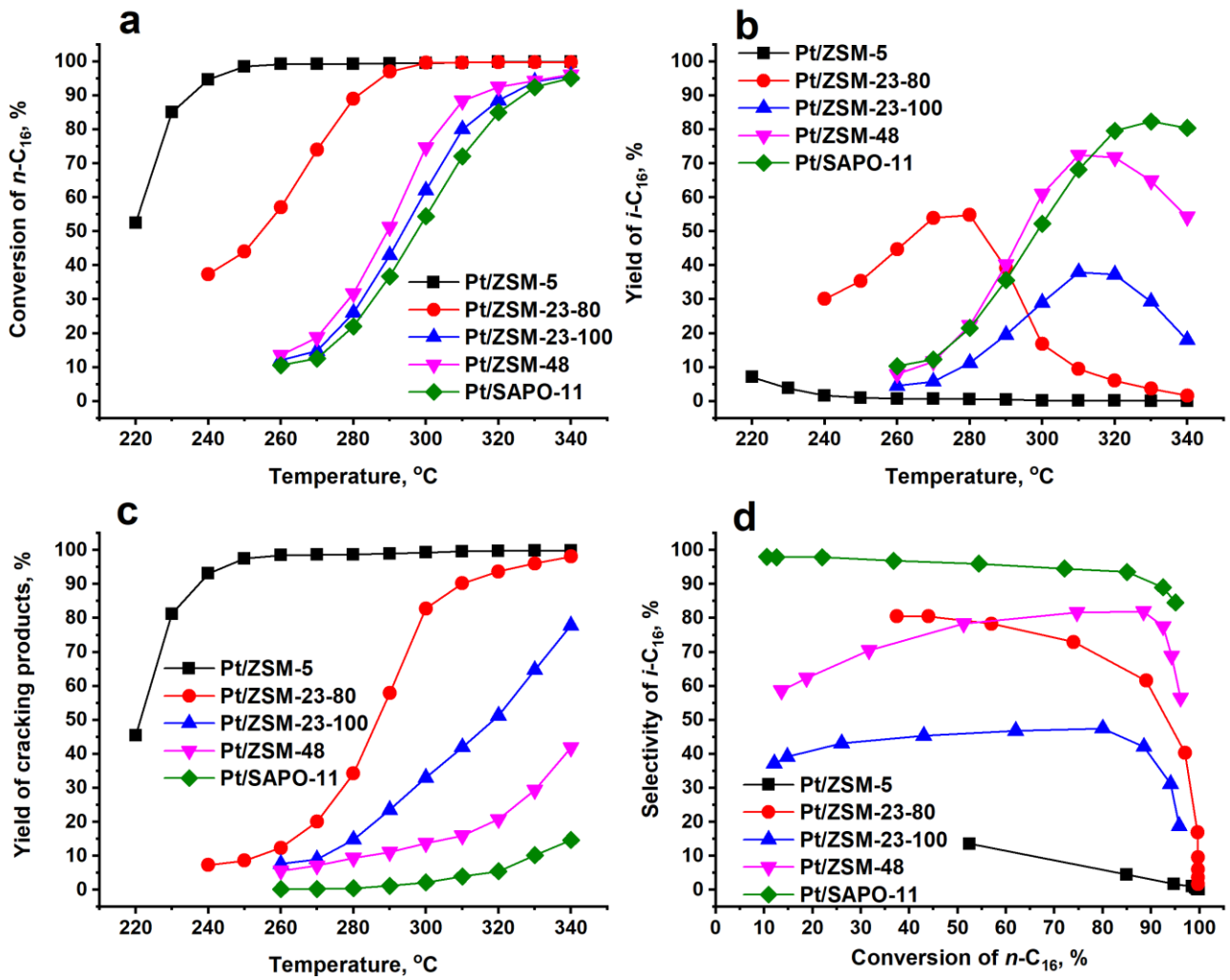

Figure 5 Hydroisomerization of n-hexadecane over molecular sieves of different structural types: (a) n-hexadecane conversion as a function of reaction temperature; (b) C_{16} isomer yield as a function of reaction temperature; (c) cracking product yield as a function of reaction temperature; (d) hexadecane isomer selectivity as a function of n-hexadecane conversion.

Firstly, its crystals are nanosized—approximately 50 nm—which drastically shortens the diffusion paths for bulky molecules like n-hexadecane and minimizes the probability of secondary transformations within the pores. Secondly, the extremely high SiO_2/Al_2O_3 ratio (140) results in a very low concentration of acid sites, most of which are weak or moderate. This "moderate" acidity is sufficient to initiate isomerization but insufficient to activate cracking reactions, which require stronger acid sites. In combination, the nanocrystalline nature and weak acidity allow ZSM-48 to efficiently direct the conversion of n-hexadecane predominantly toward the target isomers, avoiding excessive hydrocarbon chain cleavage.

ZSM-23-80, despite its one-dimensional pore structure and moderate acidity, demonstrated a more modest isomer yield. Its needle-like crystals, 200–300 nm in size, although creating a developed intercrystalline porosity, still possess a significantly longer diffusion path compared to that in the ZSM-48 nanocrystals. Furthermore, as shown by the NH_3-TPD data, the strength of its acid sites is even higher than that of ZSM-5, which, at temperatures above 280 °C, promotes not only isomerization but also partial cracking, thereby reducing the overall selectivity.

The maximum yield of C_{16} isomers over the larger-crystal ZSM-23-100 (37%) was significantly lower than that over ZSM-23-80 (55%), which is consistent with its reduced specific surface area, decreased micropore volume, and, consequently, reduced accessibility to acid sites. Thus, increasing the crystal size in the ZSM-23 series negatively impacts the catalytic performance, underscoring the critical role of nanoscale morphology in the efficient hydroisomerization of heavy paraffins.

SAPO-11, demonstrating the highest isomer yield (80%), exemplifies the classic model of an "ideal" catalyst for heavy paraffin hydroisomerization: its nanocrystals of ~200 nm size with a truncated cone morphology and a developed secondary porous structure significantly improve mass transfer, the one-dimensional channels of the AEL structure limit the degree of branching, and the weak acid sites characteristic of silicoaluminophosphates ensure high selectivity without excessive cracking activity.

ZSM-23-80, with the strongest acid sites (ammonia desorption activation energy of 225 kJ/mol), achieves the

 DOI: 10.15826/chimtech.9253

maximum isomer yield already at 280 °C, whereas ZSM-48 (215 kJ/mol), ZSM-23-100 (215 kJ/mol), and SAPO-11 (208 kJ/mol) reach their peak activity only at higher temperatures of 310–320 °C. This indicates that high acid strength facilitates the efficient activation of long-chain paraffins under milder conditions, making ZSM-23-80 a preferable catalyst for low-temperature hydroisomerization.

The differences in the ratios of monomethylpentadecanes to more branched hexadecane isomers (M/B), obtained at similar conversions of 85–90% (Table 5), are due to the combined influence of the molecular sieve topology, acidic properties, and crystal size and morphology. The three-dimensional structure of ZSM-5 (M/B = 1.1) ensures high mobility of intermediates and an absence of steric constraints, which promotes the formation of multibranched isomers and cracking. In the one-dimensional sieves (ZSM-23, ZSM-48, SAPO-11), narrow, non-intersecting channels suppress the formation of bulky carbocation intermediates, thereby increasing the M/B ratio. The highest value (2.70) observed for SAPO-11 is explained by the combination of its inherently moderate and weak acid sites, characteristic of silicoaluminophosphates, nanocrystalline size (~100–300 nm), and developed secondary porosity, which minimize secondary transformations.

ZSM-23 (M/B = 1.9), despite its one-dimensional structure, possesses stronger acid sites and a needle-like morphology that prolongs diffusion paths and promotes partial branching. ZSM-48 (M/B = 1.5) features nanocrystals (~50 nm), but, likely due to its slightly larger pore size compared to SAPO-11 coupled with its very low acid site density resulting from high SiO_2/Al_2O_3 ratio, it allows for the formation of a greater number of dimethyl-substituted isomers, thereby reducing its M/B ratio relative to SAPO-11. The mono- to dimethyl-substituted isomer ratio obtained over the larger-crystal ZSM-23-100 (M/B = 1.4) indicates a somewhat greater tendency for the formation of branched products compared to ZSM-23-80 (M/B = 1.9).

This may be attributed to its elongated diffusion paths, which promote secondary transformations even at low overall acidity. Thus, the obtained results demonstrate that the catalytic properties of 10R molecular sieves in the hydroisomerization of higher n-paraffins are determined by a combination of their physicochemical characteristics, including acidity, topology, and crystal morphology. The conclusions drawn allow for the segmentation of their application depending on the specific technological objective.

For instance, the high activity of ZSM-23-80 at relatively low temperatures makes it promising for improving the energy efficiency of the process. In turn, catalysts based on SAPO-11 and ZSM-48 are the optimal choice for achieving maximum selectivity and yield of the target isomers with a minimal contribution from the hydrocracking side reaction. At the same time, ZSM-5, possessing the highest activity, is most effective in cases where the key task is to achieve maximum conversion of the initial n-paraffins.

4. Limitations

This comparative study revealed the superior hydroisomerization performance of Pt/SAPO-11 and Pt/ZSM-48, attributing it to their one-dimensional pores, moderate acidity, and reduced diffusion path lengths.

A primary limitation of this work is its focus on a model reaction using pure n-hexadecane. Real-world diesel hydroisomerization involves more complex mixtures where the presence of sulfur and nitrogen compounds can significantly affect catalyst activity. Furthermore, the synthesis scope was confined to well-established protocols.

Therefore, the logical next step is to investigate these catalytic systems in the hydroisomerization of industrial feedstocks like diesel fuel to bridge the gap between model studies and practical application.

Table 5 Hydroisomerization of n-hexadecane over molecular sieves of different structural types at 85–90% n-hexadecane conversion.

	Pt/ZSM-5	Pt/ZSM-23-80	Pt/ZSM-23-100	Pt/ZSM-48	Pt/SAPO-11
Conversion, %	85.0	89.2	88.5	88.4	85.0
Selectivity to i-C_{16}, %	4.5	61.46	42.1	81.9	93.6
Selectivity to cracking products, %	95.5	38.5	57.9	18.1	6.4
Composition of C_{16} isomers, %					
2M	5.3	11.7	8.4	7.4	10.00
3M	14.5	11.1	8.7	8.5	11.00
4M	5.2	8.0	6.2	7.8	9.6
5M	12.1	9.9	7.5	5.8	7.3
6M+7M+8M	15.8	25.0	27.3	31.0	35.0
B	47.1	34.3	41.9	39.5	27.1
M/B	1.1	1.9	1.4	1.5	2.7

M – monomethylpentadecanes;
B - Dimethyl and higher-branched isomers;
M/B - Ratio monomethylpentadecanes to more highly branched isomers.

 DOI: 10.15826/chimtech.9253

5. Conclusions

A comparative study of bifunctional catalysts based on medium-pore molecular sieves (ZSM-5, ZSM-23, ZSM-48, and SAPO-11) in the hydroisomerization of n-hexadecane demonstrated that their catalytic properties are determined by the complex interplay of pore topology, acidic characteristics, and crystal morphology. The three-dimensional pore structure of ZSM-5 ensures high activity but leads to excessive cracking due to its high concentration of strong acid sites and lack of spatial constraints, which drastically reduces isomer selectivity. In contrast, the one-dimensional structures of ZSM-23, ZSM-48, and SAPO-11 exhibit significantly higher selectivity, attributed to their unidirectional channel pore systems that suppress the formation of multi-branched cracking intermediates.

Among them, SAPO-11 and ZSM-48 delivered the best performance, with maximum isomer yields of 80% and 73%, respectively. This results from the combination of their favorable acidic properties (inherently moderate for SAPO-11 and low-concentration for high-silica ZSM-48), high crystal dispersity, and developed secondary porosity, which minimize diffusion limitations and suppress side reactions. ZSM-23-80, possessing the strongest acid sites among the unidirectional-channel molecular sieves, achieves high activity already at 280 °C, making it promising for energy-efficient low-temperature isomerization. However, its needle-like morphology limits its selectivity compared to its nanocrystalline analogues.

Thus, the rational design of hydroisomerization catalysts requires balancing acid site strength and concentration, unidirectional pore topology, and nanoscale morphology. This balance enables precise tuning of the activity–selectivity trade-off to meet specific technological objectives, ranging from maximizing conversion to producing high-quality, low-pour-point fuels.

Supplementary materials

No supplementary materials are available.

Acknowledgments

The work was performed within the framework of the state task of the IPC UFRC RAS (topic No. FMRS-2024-0012 " Bifunctional Molecular-Sieve Catalytic Systems for the Production of Low-Pour-Point Diesel Fuels").

Author contributions

Conceptualization: D.V.S., M.R.A.
Data curation: D.V.S.
Formal Analysis: D.V.S.
Funding acquisition: M.R.A., D.Sh.S.
Investigation: D.V.S, A.I.M., A.N.K., V.Yu.G.
Methodology: D.V.S., M.R.A.
Project administration: M.R.A.
Resources: M.R.A.
Software: D.Sh.S.
Supervision: M.R.A., D.V.S.
Validation: M.R.A., D.V.S., N.A.F.
Visualization: N.A.F.
Writing – original draft: D.V.S., N.A.F.
Writing – review & editing: M.R.A., D.V.S.

Conflict of interest

The authors declare no conflict of interest.

Additional information

Author IDs:
Dmitry V. Serebrennikov, Scopus ID 57210346068;
Artur I. Malunov, Scopus ID 58772198900;
Nadezhda A. Filippova, Scopus ID 57023467900;
Denis Sh. Sabirov, Scopus ID 12799307200;
Alfira N. Khazipova, Scopus ID 6506529764;
Vladimir Yu. Gus'kov, Scopus ID 55250329800;
Marat R. Agliullin, Scopus ID 56480769400.

Websites:
Institute of Petrochemistry and Catalysis, https://icp.csic.es/;
Ufa University of Science and Technology, https://study.uust.ru/.

References

1. Karpov NV, Vakhromov NN, Dutlov EV, Sharin EA, Bubnov MA, Gudkevich IV, Koval'chuk SS, Maksimov AL, Fadeev VV, Rudyak KB, Romanov AA, Borisanov DV. Diesel fuel for use in arctic and subtropical climates. Chem Technol Fuels Oils. 2022;58(5):790–794. doi:10.1007/s10553-022-01452-x
2. Boryaev A, Yuqing Z, Ruchkina I, Rajczyk P. Control of low-temperature characteristics of motor fuels in the arctic. Transport Res Procedia. 2021;57:95–105. doi:10.1016/j.trpro.2021.09.030
3. Aljajan Y, Stytsenko V, Rubtsova M, Glotov A. Hydroisomerization catalysts for high-quality diesel fuel production. Catalysts. 2023;13(10):1363. doi:10.3390/catal13101363
4. Abdildina K, Vassilina G, Abdrassilova A, Klassen I. A, Orynbassar R, Kanapiyeva F. The role of catalyst promotive additives and temperature in the hydroisodewaxing process. Molecules. 2023;28(22):7598. doi:10.3390/molecules28227598
5. Aljajan Y, Stytsenko V, Rubtsova M, Glotov A. ZSM-48 zeolite catalysts for hydroisomerization of linear paraffins, diesel and sustainable aviation fuels production: synthesis, characterization, and application. Catalysis Rev. 2025:1–37. doi:10.1080/01614940.2025.2495547
6. Deldari H. Suitable Catalysts for Hydroisomerization of Long-Chain Normal Paraffins. Appl Catalysis A Gen. 2005;293:1–10. doi:10.1016/j.apcata.2005.07.008
7. Zhang L, Liu N, Dai C, Xu R, Yu G, Chen B, Wang N. Recent advances in shape selectivity of MFI zeolite and its effect on the catalytic performance. In: Zeolites: Advances in Research and Applications. Nova Science Publishers; 2020:11–46.
8. Teketel S, Lundegaard LF, Skistad W, Chavan SM, Olsbye U, Lillerud KP, Beato P, Svelle S. Morphology-induced shape selectivity in zeolite catalysis. J Catalysis. 2015;327:22–32. doi:10.1016/j.jcat.2015.03.013
9. Li S, Li J, Dong M, Fan S, Zhao T, Wang J, Fan W. Strategies to control zeolite particle morphology. Chem Soc Rev. 2019;48(3):885–907. doi:10.1039/C8CS00774H
10. Yadav R, Sakthivel A. Silicoaluminophosphate molecular sieves as potential catalysts for hydroisomerization

of alkanes and alkenes. Appl Catalysis A Gen. 2014;481:143–160. doi:10.1016/j.apcata.2014.05.010
11. Baerlocher C, McCusker LB, Olson DH. Atlas of zeolite framework types. Elsevier; 2007.
12. Zhang M, Long H, Fan D, Wang L, Wang Q, Chen Y, Sun L, Qi C. Synthesis of ZSM-48 zeolites and their catalytic performance: a review. Catalysis Sci Technol. 2022;12(16):5097–5109. doi:10.1039/D2CY00267A
13. Parfenov MV, Pirutko LV, Yakovlev IV, Lapina OB, Prosvirin IP, Klimov OV, Noskov AS, Kazakov MO. Role of zeolite acidity and Ni content in hexadecane hydroisomerization over Ni/ZSM-23 catalyst. Indust Engin Chem Res. 2024;63(13):5557–5572. doi:10.1021/acs.iecr.3c03574
14. Bensafi B, Chouat N, Djafri F. The universal zeolite ZSM-5: structure and synthesis strategies. A Review. Coordinat Chem Rev. 2023;496:215397. doi:10.1016/j.ccr.2023.215397
15. Hastoy G, Guillon E, Martens J. Synergetic Effects in intimate mixtures of Pt/ZSM-48 and Pt/ZSM-22 Zeolites in bifunctional catalytic chain branching of n-alkanes. Stud Surface Sci Catalysis. 2005;158:1359–1366. doi:10.1016/S0167-2991(05)80485-9
16. Yun S, Lee E, Park Y.-K, Jeong S.-Y, Han J, Jeong B, Jeon J.-K. Selective hydroisomerization of N-dodecane over platinum supported on zeolites. Res Chem Intermed. 2011;37(9):1215–1223. doi:10.1007/s11164-011-0386-8
17. Zhang M, Chen Y, Wang L, Zhang Q, Tsang C.-W, Liang C. Shape selectivity in hydroisomerization of Hexadecane over Pt supported on 10-ring zeolites: ZSM-22, ZSM-23, ZSM-35, and ZSM-48. Indust Engin Chem Res. 2016;55(21):6069–6078. doi:10.1021/acs.iecr.6b01163
18. Li H, Liu C, Wang Y, Zheng J, Fan B, Li R. Synthesis, characterization and n-hexane hydroisomerization performances of Pt supported on alkali treated ZSM-22 and ZSM-48. RSC Adv. 2018;8(51):28909–28917. doi:10.1039/C8RA04858D
19. Ge S, Hu Z, Xie H, Gao S, Zhang Z, Wu Z. Shape selection of alkane hydroisomerization over one-dimensional zeolite supported Pt catalyst: Pt/ZSM-48 versus Pt/ZSM-22. Microporous Mesoporous Mater. 2024;376:113179. doi:10.1016/j.micromeso.2024.113179
20. Zhao J, Yu H, Xu H, He Z, Shao F, Lu P, Valtchev V. Empowering catalysis and separation: morphology control of MFI zeolites using organic additives. Sustainable Energy Fuels. 2025; 9; 2:323. doi:10.1039/D4SE01514B
21. Reddy JK, Motokura K, Koyama T, Miyaji A, Baba T. Effect of Morphology and Particle Size of ZSM-5 on Catalytic Performance for Ethylene Conversion and Heptane Cracking. J Catalysis. 2012;289:53–61. doi:10.1016/j.jcat.2012.01.014
22. Meunier FC, Verboekend D, Gilson J-P, Groen JC, Pérez-Ramírez J. Influence of crystal size and probe molecule on diffusion in hierarchical ZSM-5 zeolites prepared by desilication. Microporous Mesoporous Mater. 2012;148(1):115–121. doi:10.1016/j.micromeso.2011.08.002
23. Shen Y, Le TT, Fu D, Schmidt JE, Filez M, Weckhuysen BM, Rimer JD. Deconvoluting the competing effects of zeolite framework topology and diffusion path length on methanol to hydrocarbons reaction. ACS Catalysis. 2018;8(12):11042–11053. doi:10.1021/acscatal.8b02274
24. Agliullin MR, Kolyagin YG, Serebrennikov DV, Grigor'eva NG, Dmitrenok AS, Maistrenko VN, Dib E, Mintova S, Kutepov BI. Acid properties and morphology of SAPO-11 molecular sieve controled by silica source. Microporous Mesoporous Mater. 2022;338:111962. doi:10.1016/j.micromeso.2022.111962
25. Redhead PA. Thermal desorption of gases. Vacuum 1962;12:203–211.doi:10.1016/0042-207X(62)90978-8
26. Yu R, Tan Y, Yao H, Xu Y, Huang J, Zhao B, Du Y, Hua Z, Li J, Shi J. Toward N-alkane hydroisomerization reactions: high-performance Pt–Al_2O_3/SAPO-11 single-atom catalysts with nanoscale separated metal-acid centers and ultralow platinum content. ACS Applied Mater Interfaces. 2022;14(39):44377–44388. doi:10.1021/acsami.2c11607